

ARTICLE TYPE**Probing extreme black-hole outflows on short timescales via high spectral-resolution X-ray imagers**C. Pinto*¹ | J. F. Steiner² | A. Bodaghee³ | P. Chakraborty² | M. Sobolewska² | D. R. Pasham⁴ | A. Ogorzalek⁵ | J. Zuhone² | A. Bogdan² | M. Vogelsberger⁴¹INAF, IASF, Palermo, Italy²Center for Astrophysics, Harvard & Smithsonian, Cambridge, MA, USA³Dept. of Chemistry, Physics and Astronomy, Georgia College and State University, GA, USA⁴MIT, Kavli Institute for Astrophysics and Space Research, Cambridge MA, USA⁵Goddard Space Flight Center, NASA, Cambridge MD, USA**Correspondence**

*C. Pinto, INAF - IASF Palermo, Via U. La Malfa 153, I-90146 Palermo, Italy Email: ciro.pinto@inaf.it

We investigate outflows and the physics of super-Eddington versus sub-Eddington regimes in black hole systems. Our focus is on prospective science using next-generation high-resolution soft X-ray instruments. We highlight the properties of black hole ultraluminous X-ray source (ULX) systems in particular. Owing to scale invariance in accreting black holes, ULX accretion properties including their outflows, inform our understanding not only of the closely-related population of (similar-mass) X-ray binary systems, but also of tidal disruption events (TDEs) around supermassive black holes. A subsample of TDEs are likely to transcend super-Eddington to sub-Eddington regimes as they evolve, offering an important unifying analog to ULXs and sub-Eddington X-ray binaries. We demonstrate how next-generation soft X-ray observations with resolving power $\gtrsim 1000$ and collecting area $\gtrsim 1000 \text{ cm}^2$ can simultaneously identify ultrafast and more typical wind components, distinguish between different wind mechanisms, and constrain changing wind properties over characteristic variability timescales.

KEYWORDS:

X-ray binaries, accretion, accretion disks, black hole physics, stars: winds, outflows

1 | INTRODUCTION

X-ray binaries (XRBs) are interacting stellar systems in which a compact object, typically a neutron star (NS) or black hole (BH), accretes matter from a companion star. In the Galaxy, most XRB systems appear to accrete near-or-below the Eddington limit, defined by the luminosity $L_{\text{Edd}} \approx 1.3 \times 10^{38} (M/M_{\odot}) \text{ erg/s}$, which is the critical luminosity at which outward (spherical) radiation pressure due to Thomson scattering balances gravitational attraction, for an object of mass M . At the same time, theoretical simulations have demonstrated that compact binary systems can undergo very high accretion rates up to a few orders of magnitude times the Eddington limit over timescales as long as 10^{4-5} yr . During such super-Eddington episodes, a compact object can become extremely

bright in X-rays (Rappaport, Podsiadlowski, & Pfahl, 2005; Wiktorowicz, Sobolewska, Sadowski, & Belczynski, 2015). This is because as matter accretes onto a BH, it emits a substantial portion of its rest-mass energy away. While its emission spans the electromagnetic spectrum, the spectral-energy distribution (SED) characteristically peaks in the UV and X-rays for supermassive and stellar-mass BHs, respectively. For instance, a standard, $10 M_{\odot}$ stellar-mass BH at its Eddington-limit would exhibit an X-ray luminosity of up to $\approx 10^{39} \text{ erg s}^{-1}$. Ultraluminous X-ray sources (ULXs) are defined as XRB systems whose X-ray luminosities appear to significantly exceed this limit, and constitute the brightest XRBs. While some Galactic X-ray binaries harboring either NSs or BHs may occasionally exceed this luminosity threshold (e.g., Swift J0243.6+6124 and GRS 1915+105, Done, Wardziński, and Gierliński 2004; Wilson-Hodge et al. 2018), ULX sources

are predominantly identified in external galaxies. For classification purposes, they must generally be non-nuclear to avoid potential confusion with an active galactic nucleus (AGN).

ULXs are accordingly excellent candidate systems for studying super-Eddington accretion, or conversely to identify (sub-Eddington) intermediate-mass BHs (IMBHs) with masses of $\sim 100M_{\odot} - 10^4M_{\odot}$ in the gap between the known populations of stellar-mass and SMBHs. In either instance (super-Eddington or IMBH sources), the dynamic behavior of ULXs serves as a touchstone for the growth of the supermassive black holes (SMBHs) that have been discovered at high redshift (Bañados et al., 2018). For recent reviews on ULXs see Pinto and Walton (2023) and A. King, Lasota, and Middleton (2023).

In the center of most galaxies, there is a SMBH weighing as much as several billion times the mass of the Sun. The discovery of such massive BHs at very high redshift (i.e. $z > 7$) when the Universe was young (Fan, Bañados, & Simcoe, 2023; Fan et al., 2003; Juodžbalis et al., 2023) presents a challenge for scenarios in which seed BHs of stellar-to-intermediate mass grow via accretion at Eddington-limited rates, which corresponds to an e-folding timescale of a minimum $\gtrsim 10^7$ years (Goulding et al., 2023; Jeon, Liu, Bromm, & Finkelstein, 2023; Volonteri, Silk, & Dubus, 2015). An important motivation for investigating super-Eddington accretion in XRB systems is that they readily evolve over human-accessible timescales, unlike large SMBHs.

A related phenomenon which has been the subject of much recent scrutiny are tidal disruption events (TDEs; Rees 1988), which are transient events lasting typically ~ 1 year, in which a star is tidally sheared apart as it passes sufficiently close to a SMBH in a galactic nucleus (roughly within a Hill radius). For very massive BHs, e.g. $M > 10^8 M_{\odot}$, a typical main-sequence star will be swallowed without disrupting, but for the majority of BHs below this threshold, a star can disrupt and produce a long-lived transient that decays with a characteristic timescale of $t^{-5/3}$ (or steeper; Guillochon and Ramirez-Ruiz 2013). TDE transients have been detected across the electromagnetic spectrum, predominantly in the optical and X-rays (e.g., Auchettl, Guillochon, and Ramirez-Ruiz 2017; Hammerstein et al. 2023; Sazonov et al. 2021; van Velzen et al. 2011) and in some cases also in radio (jetted TDEs, e.g. Andreoni et al. 2022). For a touchstone $1 M_{\odot}$ star fully disrupted around a $10^7 M_{\odot}$ BH, the initial accretion rate is expected to be several-times the Eddington rate, declining to sub-Eddington after several decay timescales (but see Guillochon and Ramirez-Ruiz 2015 for additional dynamical considerations which may stretch the prompt signal).

An important ubiquitous prediction of simulations of super-Eddington accretion is the presence of powerful winds, which can reach relativistic speeds (e.g., Coughlin and Begelman

2014; Jiang, Stone, and Davis 2019; Sadowski, Narayan, McKinney, and Tchekhovskoy 2014). Winds are likewise widely found in sub-Eddington accretion flows (e.g., from BH XRBs; Ponti et al. 2012), in which mechanical outflows are both slower and less powerful than expected from the super-Eddington regime. The manifestation of these outflows across the BH mass range is of particular importance given new and promising prospects for large-area high-spectral resolution ($E/\Delta E \gtrsim 1000$) X-ray facilities such as *XRISM* (XRISM Science Team, 2020), *NewAthena* (Barret et al., 2020), and NASA Probe mission concepts *LEM* (Kraft et al., 2022) and *Arcus* (Smith et al., 2022). The former three missions employ X-ray microcalorimeters in their design, which allows for non-dispersed, high-spectral-resolution imaging, and accordingly offer the capability of investigating field XRBs (including ULXs) in observations of nearby galaxies. In this paper, we describe spectroscopic signatures and physical insights to be learned about mechanical outflows from a generational leap in high-resolution X-ray spectroscopy, particularly for super-Eddington outflows.

In Section 2, we describe ULXs which serve as our primary focus for exploring super-Eddington accretion. We describe the coupling between ULXs, TDEs, and (sub-Eddington) XRBs in Section 3. In these, we demonstrate the diagnostic potential of X-ray microcalorimeter observations of nearby galaxies with reference simulations using *LEM* as our touchstone. We discuss these results in Section 5, and present our conclusions in Section 6.

2 | ULTRALUMINOUS X-RAY SOURCES

When initially identified, ULXs were widely speculated to coincide with the elusive population of IMBHs owing to their extreme luminosity and the presence of a relatively cool (~ 0.1 keV) accretion disk component in ULX spectra (Miller, Fabiano, Miller, & Fabian, 2003). Such a peak temperature would correspond to Eddington-limited accretion for a BH of several hundred M_{\odot} with bolometric luminosity $L \approx 10^{40}$ erg s $^{-1}$ (e.g., Kaaret et al. 2001). Sustained super-Eddington accretion was considered controversial (e.g., A. R. King, Davies, Ward, Fabbiano, and Elvis 2001). The field was then significantly shaken after the discovery of X-ray pulsations from the ULX M82 X-2 with *NuSTAR* (peak luminosity of $L_X \sim 2 \times 10^{40}$ erg s $^{-1}$, Bachetti et al. 2014), which unambiguously demonstrated the possibility of a highly super-Eddington (and strongly magnetized) NS. Such pulsating ULXs (PULXs) now have been identified as the engines in a total of 6 nearby of ULXs, including the hyperluminous source NGC 5907 X-1 (Israel, Belfiore, et al., 2017). These 6 ULXPs are among a group of ~ 30 ULXs with sufficient data to identify pulsations.

This suggests that the majority of ULX systems are not NSs, but this remains an open question (e.g., Rodríguez Castillo et al. 2020). It should be noted that ULXPs have not been found to exhibit spectral characteristics distinguishing them from non-pulsating ULX sources, although they seem to occupy the part of the ULX population with hardest spectra (Pintore et al., 2017).

Deep broad-band, X-ray observations with *XMM-Newton* and, later on, *NUSTAR* of nearby ULXs (~ 10 Mpc) exhibit soft spectra typified by strong curvature below 10 keV. Such curvature is inconsistent with sub-Eddington accretion spectral signatures in both stellar-mass BHs and SMBHs, and therefore favors a super-Eddington interpretation for most ULXs (e.g., Bachetti et al. 2013; Gladstone, Roberts, and Done 2009). The so-called *ultraluminous state* was then classified into two primary regimes, depending on the photon index, Γ : soft (SUL, $\Gamma > 2$) or hard (HUL, $\Gamma < 2$) ultraluminous. Two additional sub-categories are sometimes distinguished: single-peaked HUL spectra are sometimes referred to as the broadened disk regime (BD; Sutton, Roberts, and Middleton 2013), and supersoft ultraluminous states (SSUL). Numerous ULXs have been found to change from one class to another, albeit notably always exhibiting X-ray spectra that are markedly softer than seen in (sub-Eddington) Galactic XRBs. Such variations are possibly attributed to variability of the geometry or in the outflow rate with changing obscuration of the inner accretion flow (Middleton, Heil, Pintore, Walton, & Roberts, 2015). Indeed, trends between the temperature and the bolometric luminosity of the blackbody-like components fitted to ULX spectra often deviates from the $L \propto T^4$ predicted for thin disks with characteristic peak temperature T (e.g., Steiner et al. 2010), sometimes even appearing inverted as expected from emission by an expanding photosphere or an optically-thick wind (see, e.g., Barra et al. 2022; Robba, Pinto, Pintore, et al. 2021; Walton et al. 2020).

At present, the known population of ULX candidate sources numbers ~ 2000 systems (Walton et al., 2022). Among these, perhaps the best candidate for an IMBH-hosting ULX is the hyper-luminous source (HLX-1) in ESO 243-49 (Farrell, Webb, Barret, Godet, & Rodrigues, 2009) which exhibits outbursts and spectral states that appear very similar to those seen in Eddington-limited Galactic BH XRBs. With a peak luminosity of 10^{42} erg s $^{-1}$, it would then be expected to have a mass of $10^{4-5} M_{\odot}$. Recent time delays identified between its outbursts indicates that it may be a failed TDE (Lin et al., 2020). Further evidence supporting the presence of a sub-population of IMBHs within the ULXs was provided by the discovery of timing features in a few nearby ULXs, including quasi-periodic oscillations (QPOs) with the most robust detection in M 82 X-1 (Pasham, Strohmayer, & Mushotzky, 2014). At the same time, we note that QPO frequencies in ULXs are not always

correlated with the continuum noise break frequencies and the spectral parameters (Middleton, Roberts, Done, & Jackson, 2011). A more robust indicator would be the high-frequency break in the power density spectrum (PDS, see e.g. Remillard and McClintock 2006) which is difficult to detect due to the low statistics above 0.1 Hz in most ULXs observed with currently-available instruments.

Several ULX binary companion stars have been identified using observations with *Hubble Space Telescope (HST)* in the optical and with *VLT / X-shooter* in the infrared. They appear to be primarily red or O-B supergiants, or else Wolf-Rayet stars (Gladstone et al., 2013; Heida et al., 2019). Accordingly, they are very likely fueled at least in part by powerful *stellar* winds (Wiktorowicz et al., 2021).

Blueshifted outflows from ULXs have recently been unambiguously identified in high-resolution grating spectra (e.g. Kosec, Pinto, Fabian, and Walton 2018; Kosec, Pinto, Walton, et al. 2018; Pinto et al. 2017; Pinto, Middleton, and Fabian 2016). Such features were previously spotted in low-resolution CCD spectra (e.g. Middleton, Walton, et al. 2015; Stobbart, Roberts, and Wilms 2006; Sutton, Roberts, and Middleton 2015) and also in Galactic transient ULX Swift J0243.6+6124 (van den Eijnden et al., 2019).

Evidence suggests that such outflows are present in most high-resolution ULX spectra, given their prevalence in data with sufficient counting statistics ($\gtrsim 5000$ counts; e.g. Brightman et al. 2022; Kosec et al. 2021; Walton et al. 2016). Both the outflow blueshift and ionization state appear to increase in step with X-ray spectral hardness, which aligns with a super-Eddington interpretation in which different lines-of-sight (LOS) through a conical radiatively-driven disk wind are sampled (e.g., Kobayashi et al. 2018). In this picture, the outflow obscures the innermost accretion flow at high inclinations (Pinto, Mehdipour, et al., 2020).

Notably, these winds are quite powerful, with a kinetic power comparable to the ULX electromagnetic luminosity. Accordingly, they are plausibly responsible for ~ 100 -pc bubbles of hot interstellar gas that have been identified surrounding many ULXs (Gúrpidé, Parra, Godet, Contini, & Olive, 2022; Zhou, Feng, & Bian, 2023). The enormous enthalpy of a ULX bubble is comparable to the energy released in a supernova explosion (see, e.g., Pakull, Grisé, and Motch 2006; Pinto, Mehdipour, et al. 2020), demonstrating the important role super-Eddington winds in ULXs may play as an important source of feedback affecting star formation and galaxy evolution over cosmic time.

There are several open questions regarding the properties of ULXs and, more generally, of super-Eddington accretion (for related discussion on TDEs see Sect. 3). Large uncertainties in the outflow rate and the mass loss translate into loose constraints on the net accretion (growth) rate of the compact

object. The resolution to this question bears on the kinetic mass-loss rate and the associated feedback onto the surrounding environment. Although radiation pressure is sufficient to account for the observed winds, the role of magnetic fields remains unclear. At present, no operating or adopted X-ray telescope can detect and resolve spectral lines in ULXs on critical timescales comparable to those of variations in the underlying continuum ($\lesssim 10$ ks; e.g. Alston et al. 2021; Heil, Vaughan, and Roberts 2009; Kara et al. 2020; Pinto, Walton, et al. 2020; Pintore et al. 2021). Understanding the coupling (continuum) spectral and wind variations is key to understanding the relevant physics. Until such timescales are resolved, inferences on the wind solid angle and launching mechanism, and the spectral transitions will be significantly hampered by model degeneracy. For instance, D’Ai et al. (2021) show how SUL \leftrightarrow SSUL transitions in NGC 247 ULX-1 can be successfully explained invoking either the propeller mechanism, or else wind obscuration (see also Feng, Tao, Kaaret, and Grisé 2016; Urquhart and Soria 2016). A similar issue was reported by Walton et al. (2020) for transitions between harder spectra (HUL \leftrightarrow BD) in NGC 1313 X-1. Such ambiguity prevents us from distinguishing between accretion disks dominated by magnetic versus radiation pressure. Importantly, principal component analysis (PCA) of the *XMM-Newton* CCD spectra proved evidence of variability in the wind on 10 ks timescales in both ULXs (e.g., Pinto, Walton, et al. 2020) and highly-accreting SMBHs (e.g., Parker, Reeves, Matzeu, Buisson, & Fabian, 2018; Xu et al., 2022). Accessing these fast timescales is important in understanding the wind response to the source continuum and, ultimately, the launching mechanism of the wind. In consideration of these issues, we below describe case-studies of NGC 1313 X-1 and NGC 247 ULX-1 for a telescope with effective area $\gtrsim 1000$ cm² and spectral resolution of about 1 eV, corresponding to a resolving power of 1000 around 1 keV, and how such capabilities can deliver key insights on critical timescales and revolutionize this field.

2.1 | Spectral simulations

2.1.1 | NGC 1313 X-1

To assess the prospects of next-generational high-resolution spectrographs for diagnosing outflow signatures in ULXs, we consider the archetypal ULX NGC 1313 X-1, for which we simulate a HUL spectrum adopting the plasma model described in Pinto, Walton, et al. (2020) which consists of a multiphase wind in emission and absorption. We are principally interested in the rich suite of low-energy line features ($\lesssim 1$ keV) and accordingly adopt a *LEM*-like instrument with an assumed 1 eV energy resolution over a spectral range of 0.2-2 keV, with a peak effective area ~ 2500 cm² at 1 keV.

A 10 ks simulated observation is performed with SPEX code (Kaastra, Mewe, & Nieuwenhuijzen, 1996), which is state-of-the-art for photoionized plasmas, with the primary goal of probing the properties of the wind on the variability timescales discussed above. The continuum emission adopted is a standard super-Eddington ULX model consisting of one cool (0.2 keV) and another hot (2 keV) blackbody-like thermal components, plus a powerlaw with a hard photon index $\Gamma = 0.59$ and a typical low-value for the high-energy cutoff $E_{\text{cut}} = 7.9$ keV as described in Walton et al. (2020). The multiphase, hybrid, wind model predicts features of collisionally-ionized gas (at rest) in emission (CIE) and photoionized gas in absorption (PION) which is blueshifted by $0.2c$ (see Pinto, Walton, et al. 2020). The model thus consists of one CIE component in emission and one PION component in absorption, by which the continuum is multiplied.

Our results show that the line-emitting and absorption plasma would contribute $\Delta\chi^2 \sim 100$ each, which corresponds to detection levels well above 5σ , accounting for the *look-elsewhere* (LE) effect (see, e.g., Pinto et al. 2021). The uncertainties predicted for the ionization parameter and the column density will be of the order of 10-20% (and even smaller for the velocities, ~ 100 km s⁻¹), which is remarkable for such a short timescale. To readily visualise the detection of the most crucial absorption features, we performed an automated multi-dimensional scan on a suite of such simulated spectra while making use of grids of photoionization models. The results are shown in Fig. 1 (right panel). This plot was produced by removing the photoionized absorber from the model and scanning grids of absorbers throughout a large parameter space with steps of ($\Delta \log \xi = 0.2$, $\Delta v_{\text{LOS}} = 500$ km s⁻¹ and v_{disp} fixed to 1000 km s⁻¹).

As a bottom line, winds in a statistical number of ULXs could be readily detected at timescales of just a few ks. Notably, this is comparable to the timescale of lags observed in this and in other ULXs (see, e.g., Heil et al. 2009; Kara et al. 2020; Pinto et al. 2017; Pintore et al. 2021) thereby providing a **novel means of determining the disk-wind structure** and its coupling to the spectral transitions commonly observed in ULXs (HUL \leftrightarrow BD \leftrightarrow SUL \leftrightarrow SSUL). Such line diagnostics achieved here are presently out of reach for current facilities. For instance, the gratings on *XMM-Newton* and *Chandra* would require exposure times > 300 ks to achieve 5σ line detections for nearby ULX systems (see, e.g., Kosec et al. 2021 for a representative study). Even *XRISM* Resolve would need ~ 100 ks to achieve $\sim 5\sigma$ line detections, nevertheless a 3-times improvement over gratings instruments (e.g. Pinto and Walton 2023). Notably, because most spectral features are at lower energies around 1 keV, and given that photon fluxes are high at lower-energies, a *LEM*-like instrument would offer an

order of magnitude increase in line sensitivity for characteristic ULX spectra which promises to be transformative for our understanding of super-Eddington accretion.

Although the simulated 10 ks observation is sufficient to measure and track changes of the wind column density, ionization parameter and velocities, deeper observations might be needed to constrain the volume density (n_e), a parameter which is now elusive in all ULX spectra. We therefore performed another simulation adopting a *LEM*-like instrument and 100 ks exposure time. The simulated spectrum is shown in Fig. 1 (left panel) in which the template model is overlaid as a solid red line. Many emission lines are detected above a 10σ confidence level. The O VII He-like triplet around 22 \AA is detected with such a high quality that the relevant line ratios $r(n_e) = F/I$ and $g(T_e) = (F + I)/R$, are determined with uncertainties below 20% and 40%, respectively, where F, I and R are the fluxes of the forbidden, intercombination and resonance lines. Such precision is essential to place tight constraints on the elusive density parameter (see, e.g., the case-study of the Galactic XRB EXO 0748-676 in Psaradaki, Costantini, Mehdipour, and Díaz Trigo 2018).

Crucially, this precision is sufficient to **discriminate the ionization mechanism, e.g. photoionization vs. collisional**, of the line-emitting plasma. For comparison, an alternative model of a pure photoionization plasma (i.e., consisting of PION components both in emission and absorption) is shown as a solid black line in Fig. 1 (left panel, for more detail see Pinto, Walton, et al. 2020). It is clear that such a model would predict a much stronger emission around 1 keV from Ne and Fe ionic species compared to the hybrid plasma. Distinguishing between collisional and photoionization models is key to understanding whether the wind is driven by radiation as well as to constraining the role of outflows in producing the large bubbles surrounding numerous ULXs (e.g., Gúrpide et al. 2022; Pinto, Mehdipour, et al. 2020).

The strongest (blueshifted) absorption features from O VIII and Fe XIX-XX at 15.9 and around 11 \AA are detected at $8-9\sigma$. Even after accounting for the LE effect, this would constitute a detection significance 5σ each, providing accurate measurements of the relevant parameters (column density $N_{\text{H}} = 2.0 \pm 0.1 \times 10^{21}\text{ cm}^{-2}$, log-ionization parameter $\log(\xi/\text{erg s}^{-1}\text{ cm}) = 2.40 \pm 0.02$, velocity dispersion $v_{\text{disp}} = 1000 \pm 80\text{ km s}^{-1}$, LOS velocity $v_{\text{LOS}} = -52500 \pm 80\text{ km s}^{-1}$). This is crucial to **measuring the outflow and kinetic rates with high accuracy**, which establish the feedback energetics. To be responsible for producing the observed bubbles, a kinetic rate above $10^{39}\text{ erg s}^{-1}$ is required. Absorption features produced by the intervening interstellar medium along the LOS manifest prominently, especially Fe-L and O-K neutral edges near 17.5 and 23 \AA (for oxygen the 1s-2p line is also detected), which enables detailed study of the interstellar chemical composition along the LOS

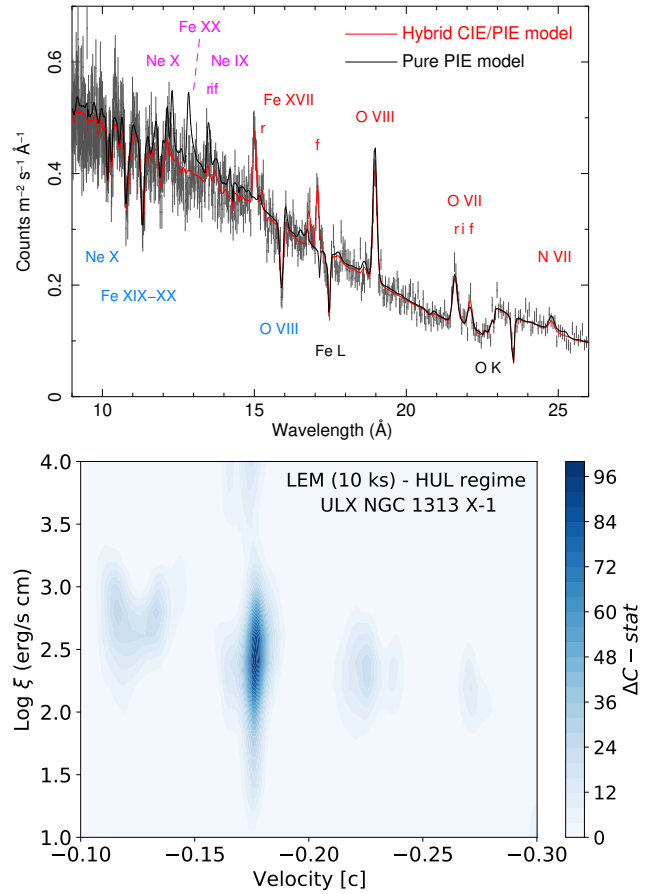


FIGURE 1 Left panel: *LEM*-like 100 ks simulated spectrum for the HUL regime of ULX NGC 1313 X-1 for a hybrid, ionized, wind model (data in grey, model as a solid red line). Overlaid is pure-photoionization model in black. The energy centroids of the strongest emission (at rest) and absorption lines (blueshifted by about $0.2c$) are labelled. The “r,i,f” refer to resonance, intercombination and forbidden emission lines. Right panel: photoionization absorption model scan for a *LEM*-like 10 ks simulation of NGC 1313 X-1 HUL spectrum plotted in the 2D parameter space of velocity and ionization parameter, ξ . The LOS velocity is in units of the speed of light. Negative values indicates blueshifts, i.e. motion in the direction of the observer. The color is coded according to the spectral fit improvement with respect to the continuum model. The 2D plot shows that we will be able to follow wind changes on timescales shorter than 10 ks and to study the disk-wind connection.

in the host galaxy (in particular, elemental abundances and dust fractions, Pinto, Kaastra, Costantini, and de Vries 2013; Psaradaki et al. 2023); such measurements are not possible with present facilities.

of magnitude in luminosity. Narrow-line Seyfert 1 galaxies (NLS 1) have BH masses in the range $10^{6-8} M_{\odot}$ and accretion rates that can surpass the Eddington limit by a factor of up to 10. Unsurprisingly, these commonly exhibit prominent and powerful winds (e.g. Komossa et al. 2006). TDEs are generally discovered via new activity for a previously quiescent SMBH. Their X-ray spectra are typically very soft (blackbody temperatures below 0.1 keV) as in some NLS 1 but with possibly higher accretion rates (up to a hundred-fold, e.g., Wu, Coughlin, and Nixon 2018) analogous to ULXs (Komossa, 2015). NLS 1 and TDEs may therefore represent the “supermassive counterparts” to ULXs (Dai, McKinney, Roth, Ramirez-Ruiz, & Miller, 2018). Most interestingly, given their relatively short (months-to-years) evolution timescales, TDEs provide a unique means to follow an evolution of accretion from an initial super-Eddington phase (for large stellar-disruptions around undermassive SMBHs), through sub-Eddington phases and back to quiescence. Notably, TDEs can also exhibit shorter timescale variability on a \lesssim day-long timescales (see, e.g., Pasham et al. 2019; Pasham and van Velzen 2018). In particular, one very bright TDE that occurred in a nearby galaxy (ASASSN-14li, at only 90 Mpc) offered uniquely rich, high-resolution spectra taken with *XMM-Newton* and *Chandra* gratings (about 40 ks each) which showed strong absorption lines blueshifted by about 100 km s^{-1} , either due to circulating streams or radiation-driven winds (Miller et al., 2015). Further evidence of outflows at even higher velocities was provided by CCD spectra (Kara, Dai, Reynolds, & Kallman, 2018).

Grating spectrometers enable the detection of narrow features from TDEs but require long exposures, > 10 ks for the closest TDEs, and becoming prohibitively long for TDEs at high redshift ($z > 1$). The lack of a combined high spectral-resolution and large effective-area facility inhibits an ability to track the plasma evolution on the requisite dynamical timescales which would distinguish between circulating streams vs. outflows ($\lesssim 1$ ks for a $10^6 M_{\odot}$ SMBH). On the other hand, because broad features detected with CCDs near 1 keV are unresolved, we are missing unambiguous proof of UFOs in TDEs that would be definitive in revealing the role of radiation pressure in super-Eddington disks, mass loss, and feedback.

3.1 | Spectral Simulations

In this section we present *LEM*-like spectral simulations of a TDE. Notably, the results here equally have bearing on other high-resolution spectroscopic studies of SMBHs, particularly those with lower mass ($\lesssim 10^8 M_{\odot}$) and high accretion rate ($\dot{M} \gtrsim 0.1 \dot{M}_{\text{Edd}}$) such as NLS 1. We use the case of ASASSN-14li as a benchmark for our simulation, based upon the results of (Miller et al., 2015). The presence of a broad, P Cygni-like

absorption feature at around 0.7 keV found in low-resolution *XMM-Newton* CCD spectra of ASASSN-14li intriguingly suggests the presence of relativistic outflows ($v_{\text{LOS}} \sim 0.2c$, Kara et al., 2018). Modeling and discerning these outflow components is crucial to estimating the mechanical feedback on the immediate environment of the SMBH with potential ramifications for nuclear star formation. Plasma flows have been shown to be multiphase in both stellar-mass compact objects such as XRBs and ULXs (e.g., Miller et al. 2016; Pinto, Walton, et al. 2020) as well as persistent AGN (e.g., Mizumoto, Nomura, Done, Ohsuga, and Odaka 2021; Xu et al. 2021) and, more recently, in TDEs (Kosec, Pasham, Kara, & Tombesi, 2023).

We initially simulate 10 ks observations using the *LEM*-like instrument above and demonstrate that it will be trivial to assess any plasma (and continuum) variability for another ASASSN-14li throughout the TDE evolution over month-timescales. We employed the best-fitting models for the grating spectra in sequential epochs from Miller et al. (2015). The simulated spectra are shown in Fig. 3 (left panel). Several individual lines can be identified in each spectrum which provide an unprecedented view of the plasma properties for a TDE. The time evolution of the plasma, such as its LOS velocity can be measured with uncertainties of about 10 km s^{-1} , which **provides the means to distinguish between dynamical circulation of streams around the SMBH** (periodic and both red- and blueshifts) **versus outflows** (more chaotic with predominantly blueshifted absorption lines).

Previously, it was shown that the X-ray continuum of TDEs vary on short timescales of 1 ks or less (Pasham et al. 2019). We therefore explore a short snapshot simulation of 1 ks to test whether the data quality would allow detection and characterisation of both the low- and high-velocity plasma flows. This was done by adopting the RGS continuum model for an *XMM-Newton* observation (ID: 0722480201) and adding two PION components with the best-fit parameters for the slow-motion and ultrafast outflows (Kara et al., 2018; Miller et al., 2015). The two PION components were then removed from the model and the data was refitted through a loop of model grids of PION within a large parameter space (assuming a velocity dispersion of 100 km s^{-1}).

For this scan we use the same code used to produce Fig. 1 (right panel). The results for ASASSN-14li are shown in Fig. 3 (right panel). Both the close-to-rest and ultrafast components of the plasma are easily detected with large significance, well-beyond the 5σ confidence level threshold. The predicted uncertainty for parameters of interest such as the ionization parameter and the LOS velocity are very small ($\Delta \log \xi \sim 0.1$ and $\Delta v_{\text{LOS}} \sim 30 \text{ km s}^{-1}$), which is sufficient to track changes in the plasma and its response to variations in the underlying

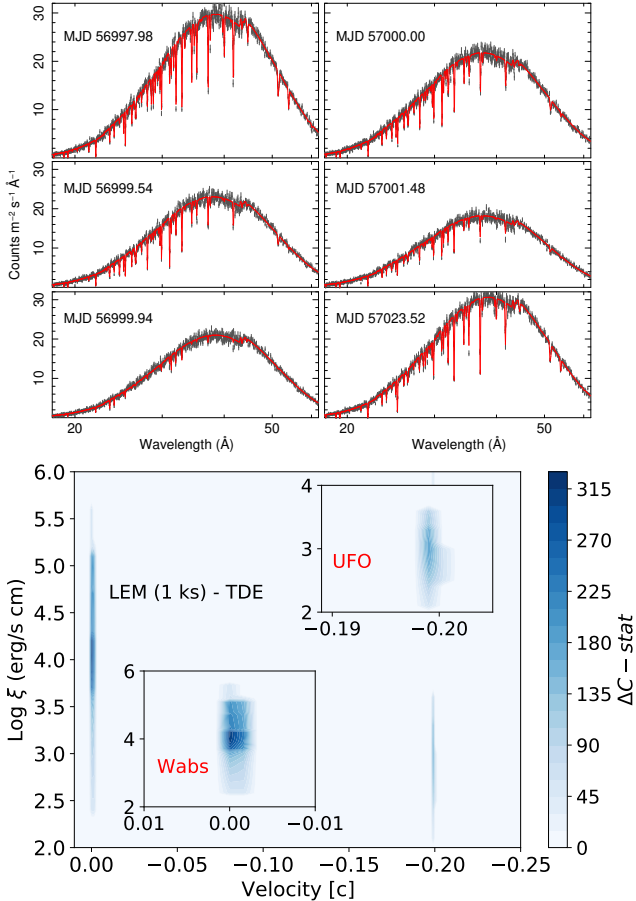


FIGURE 3 Left panel: time evolution of ASASSN-14li as it would be seen with a *LEM*-like instrument. Exposure times of 10ks and the spectral models from Miller et al. (2015) were adopted. Right panel: contour plots of spectral improvement from a photoionized absorber with respect to the continuum model for a 1 ks *LEM*-like observation simulated for ASASSN-14li (based on obs. ID: 0722480201). Both the slow-motion gas (Miller et al., 2015) and the ultrafast outflow (Kara et al., 2018) are detected and resolved with very high confidence. The strength of such signals readily enables dynamic monitoring of wind evolution in TDEs over their characteristic timescales of days and longer, e.g., as a system may transition from super-to-sub-Eddington regimes, viz. a motion-picture of the right-hand panel portraying time variance of the component wind strength and speed.

continuum on timescales less than an hour. Accordingly, next-generation facilities will unambiguously prove the presence or absence of claimed UFOs in TDEs.

3.1.1 | High-redshift TDEs

We now perform a detailed spectral simulation a bright TDE for a range of redshifts while taking into account the effects of absorption from winds as done above for ASASSN-14li. On this basis, in Section 4.1 we will consider prospects for a potential background TDE with $L_X \sim 10^{44}$ erg s⁻¹ during a putative deep observation of a nearby galaxy.

Here, we again adopt the best-fit obtained for ASASSN-14li’s spectrum taken from *XMM-Newton* / RGS (Miller et al., 2015). We have considered several cases with the redshift increasing from 0.02 to 1.5. As for the simulations shown in Fig. 3, we adopted a blackbody continuum model with (fixed) bolometric (1.24–124 Å) luminosity of 2.2×10^{44} erg s⁻¹ and temperature 51 eV. The absorber was modeled with a PION component assuming an ionization parameter $\log \xi = 4.1$, a velocity dispersion $v_{\text{RMS}} = 110$ km s⁻¹, an outflow velocity $v_{\text{LOS}} = -210$ km s⁻¹ and a column $N_{\text{H,PION}} = 1.3 \times 10^{22}$ cm⁻². The Milky Way ($N_{\text{H,MW}} = 2.6 \times 10^{20}$ cm⁻²) and host ($N_{\text{H,HG}} = 1.4 \times 10^{20}$ cm⁻²) absorption is also taken into account.

In Fig. 4 we show the expected spectrum at redshifts of 0.1, 0.5 and 1.0 (for exposure times of 20 ks, 200 ks and 500 ks, respectively). The photoionization signatures of the plasma are readily detected at $z \sim 0.1$ (mainly through absorption lines of C VI, N VI-VII, O VII-VIII and some heavier species), whereas by $z \gtrsim 0.5$ heavy binning is required to achieve enough signal, which thereby smears the features. In brief, a TDE (or similarly bright supersoft source) would be **easily detectable up to redshift ~ 1** . From $z \gtrsim 1.2$ the source spectrum would be significantly hampered by the background. **For nearby TDEs at $z \lesssim 0.1$ it would be trivial to trace changes in the outflow properties** across a > 10 -fold decline in the luminosity.

4 | XRB POPULATIONS IN NEARBY GALAXY OBSERVATIONS

High spectral-resolution wide-field X-ray imagers such as *XRISM/Resolve*, *NewAthena/X-IFU*, and *LEM* are poised to do wide-ranging science involving long observations of nearby galaxies (within ~ 20 Mpc). Such objectives may include investigating AGN feedback (e.g., Fabian 2012), characterizing the circumgalactic medium (Schellenberger et al., 2023), studying extragalactic X-ray binary populations (Lazzarini et al., 2018), measuring AGN reverberation or variability (e.g., Cackett, Bentz, and Kara 2021), or searching for faint ionization cones around AGN jets (J. Wang et al., 2011). Regardless of the primary aim, winds from *all* sufficiently-bright X-ray binaries and ULXs will be a science byproduct of long stares at their host galaxies. Below, we consider one such example

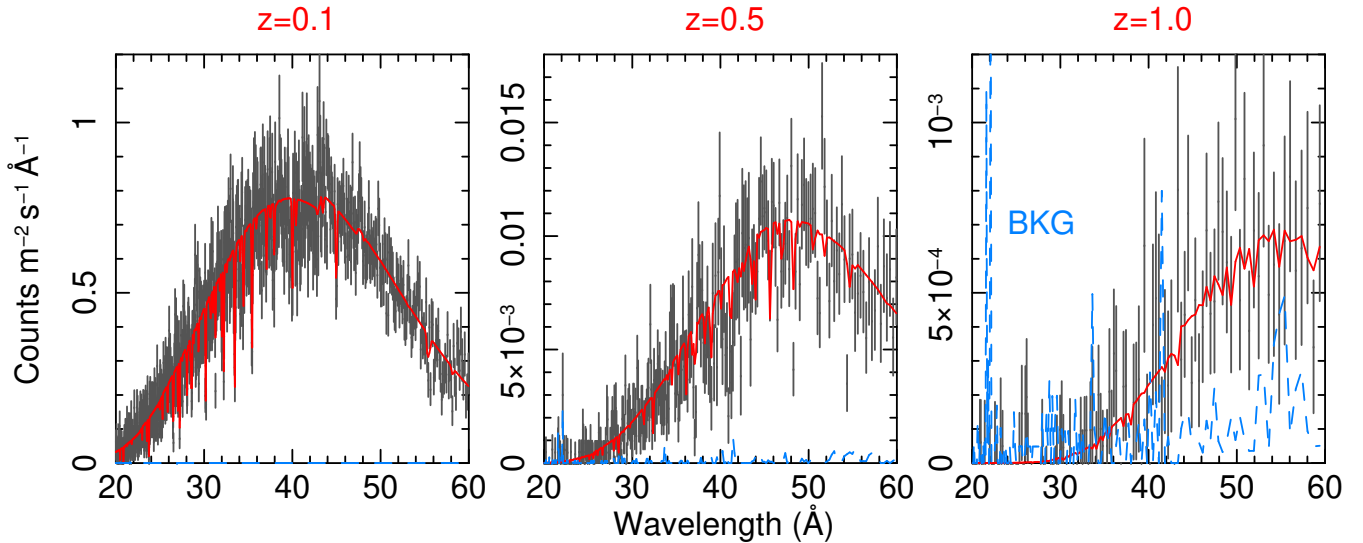


FIGURE 4 *LEM*-like instrumental simulations of TDE ASASSN-14li-like TDEs for a range of redshifts. The data (grey) are simulated with the model (red) accounting for photoionized absorption. Exposure times of 20 ks, 200 ks and 500 ks were adopted, respectively, for redshifts increasing from 0.1 to 1.0.

to highlight typical results for outflows in accreting black-hole systems for field X-ray binaries and ULXs. This is quite notable because presently, only extreme winds in individual ULXs can be studied, and there requiring substantial *dedicated* observing time.

4.1 | M 83 field of view end-to-end simulation

M83 is a face-on spiral galaxy situated relatively close to the Milky Way ($d = 4.5$ Mpc) in a direction with little photoelectric absorption ($N_{\text{H}} = 4 \times 10^{20} \text{ cm}^{-2}$, Kalberla et al., 2005). Deep *Chandra* observations show that M83 hosts around 200 XRBs of which 120 are likely high-mass X-ray binaries (HMXBs), 30 are likely low-mass X-ray binaries (LMXBs), and the remaining are either of intermediate mass or unclassified XRBs (Hunt et al., 2021). This combination of attributes makes M83 an ideal touchstone source with which to study how massive stars evolve in relation to their host galaxy (e.g., Lehmer et al., 2019).

We simulate an observation of M83 for a *LEM*-like instrument for the same spectroscopic specifications described above, assuming $15''$ pixels and a $30' \times 30'$ field of view for imaging capabilities. We first selected all point sources from the *Chandra* catalog of Long et al. (2014) that are located less than 0.1 deg from the center of M83 (~ 13 kpc at this distance), with an X-ray luminosity $\geq 10^{37} \text{ erg s}^{-1}$ (0.35–8 keV). These 77 sources were modeled in the same manner as in Long et al. (2014), i.e., assuming a power law spectrum ($\Gamma = 1.9$) with photoelectric absorption through the Milky Way ($N_{\text{H}} = 4 \times 10^{20} \text{ cm}^{-2}$).

The *Chandra* image (Fig. 5 ; left panel) reveals that M83 contains complex diffuse emission in addition to a constellation of point sources. An image isolating this diffuse emission was created by filtering out all ~ 450 point sources listed in Long et al. (2014) with the CIAO tool `dmfilth` using bilateral interpolation. The spectra of this residual emission was then modeled as was done for the inner and outer disk of M83 by Q. D. Wang, Zeng, Bogdán, and Ji (2021): i.e., an APEC ($T = 0.1$ keV) for the ionized gas and a power law ($\Gamma = 1.9$) to account for unresolved background AGN, both of which are attenuated by the Milky Way’s column density ($N_{\text{H}} = 4 \times 10^{20} \text{ cm}^{-2}$), for a total flux of $1.3 \times 10^{-12} \text{ erg cm}^{-2} \text{ s}^{-1}$ (0.5–2 keV).

Spectral models for the point sources and diffuse emission, as well as the diffuse image, the instrumental background, and response matrix files, were used as inputs to SOXS¹ which was used to generate event and image files. An exposure time of 700 ks was chosen to be similar to that of the *Chandra* exposure. Figure 5 (right panel) presents the simulated *LEM*-like image. Despite poorer spatial resolution, individual XRBs are readily resolved in the spiral arms and disk.

For example, consider the brightest of the two LMXBs labeled in Fig. 5 , which is listed as X299 in Long et al. (2014). With $L_{\text{X}} = 2.2 \times 10^{39} \text{ erg s}^{-1}$ (0.35–8 keV), X299 is more than twice as bright as any other object in the catalog and a candidate ULX. Simulations show that a *LEM*-like instrument can easily constrain the spectral parameters for simple models such as an absorbed power law ($N_{\text{H}} = [4.5 \pm 0.4] \times 10^{20} \text{ cm}^{-2}$; $\Gamma = 1.94 \pm 0.02$). Better still, wind models which include

¹<https://hea-www.cfa.harvard.edu/soxs/>

absorption and emission lines can be readily fitted to achieve wind diagnostics analogous to those in Section 2.1 for field ULXs and sub-Eddington XRBs.

After ULXs, active BH XRB systems are the brightest non-nuclear sources in a galaxy. Such systems, which here we are distinguishing from ULXs, accrete at sub-Eddington limits and exhibit a ranges of spectral-timing states, which are typically characterized as hard or soft (e.g., Fender, Belloni, and Gallo 2004; Remillard and McClintock 2006). These are dominated, respectively, by nonthermal coronal emission, and thermal disk radiation. High luminosities are typically associated with soft states. BH XRBs show stronger outflows associated with soft states (e.g., Ponti et al. 2012), and it has been suggested that there is tradeoff between the mass flow in winds and that in a compact jet (Nielsen & Lee, 2009). At the present, the properties of winds across the transition from super-Eddington to sub-Eddington regimes remains largely unconstrained observationally, and it is e.g., unclear whether a single wind mechanism dominates at all accretion rates, or if this varies with state and luminosity.

A powerful magnetically-driven wind was observed during an unusual “hypersoft” state for the bright Galactic BH XRB GRO J1655-40 (Miller et al., 2008). Remarkably, as shown in Fig. 6, with microcalorimeter imagers capable of discerning point sources in nearby galaxies, dozens of comparably high-quality spectral data can be obtained simultaneously for an entire extragalactic field in a single long observation!

5 | DISCUSSION

Microcalorimeter spectrometers are expected to boost our sensitivity to weak lines. The sensitivity can be defined as the ratio between effective area and energy resolution or $A_{\text{eff}}/\Delta E$. The grating spectrometers onboard *XMM-Newton* (RGS) and *Chandra* (HETGS and LETGS) have been operated for over twenty years and enabled line detection of bright sources ranging down to a 0.3-10 keV flux $\sim 10^{-11}$ erg s $^{-1}$ cm $^{-2}$ (the faint-end of which requires observations of 100 ks or longer). This has been essential to detect flows of hot plasmas within different environments (compact objects, interstellar medium, etc). The X-Ray Imaging and Spectroscopy Mission (*XRISM*, Guainazzi and Tashiro 2018) launched in September 2023 bears the Resolve microcalorimeter ($\Delta E \sim 5$ eV and PSF $\sim 1'$), which is 10 times more sensitive than the gratings aboard *XMM-Newton* and *Chandra* above 4 keV but around 0.7 keV is comparable to the RGS. Simulations equivalent to those that in Sect. 2.1 have shown that *XRISM* can provide a better view of the hotter wind phases but in such cases $\gtrsim 100$ ks observations are needed, even for the brightest ULXs at distances of 4-5 Mpc (Pinto, Mehdipour, et al., 2020).

Next-generations microcalorimeters like *LEM* (Kraft et al., 2022) and (*New*)*Athena*’s X-ray Integral Field Unit (X-IFU) (Barret, Lam Trong, den Herder, Piro, et al., 2018) offer comparable and leading sensitivity, with *LEM* offering higher spectral resolution and a significantly larger FOV, while the X-IFU offers a balancing larger effective area, and with energy coverage at higher energies. Both facilities would enable us to access much shorter timescales as shown in Sect. 2.1 and 3.1. In Fig. 7, we qualitatively show the shortest measurable timescales (smallest exposure times) required to detect lines at high confidence levels (i.e. $\sim 5\sigma$). For dedicated X-IFU simulations of the wind detection in NGC 1313 X-1 we also refer to Pinto, Mehdipour, et al. (2020). Interestingly, *LEM* is the most sensitive choice for the softest sources such as TDEs and soft-ULXs (SUL), whereas X-IFU is the more sensitive for harder spectra and very high ionizations, e.g. in hard-ULXs (HUL) and classical XRBs (with the exclusion of the hypersoft states).

In the following we examine several driving science questions on the accreting BH systems we have considered and describe implications of our simulations on these issues. We first consider timing capabilities as a means of distinguishing the nature of a ULX host. We next examine constraints on the donor star attributes, both in the cases of stellar-mass (XRB) and supermassive (TDE) accretors. We then consider geometrical and inclination effects associated with the disk-wind structure at super-Eddington rates. Finally, we explore implications for the growth of BHs and the mechanical feedback associated with compact objects at different mass scales.

5.1 | Spectral-timing properties of BHs with *LEM*

Timing features such as pulsations, QPOs, and PDS breaks, can be best revealed by traditional Fourier-domain methods (e.g., Kelly, Becker, Sobolewska, Siemiginowska, & Uttley, 2014). As described in Sec. 2, these features were instrumental in demonstrating that the compact objects in ULXs form a heterogeneous class, which includes exotic cases such as super-Eddington accreting NSs (Bachetti et al., 2014; Carpano, Haberl, Maitra, & Vasilopoulos, 2018; Fürst, Walton, Harrison, et al., 2016; Israel, Belfiore, et al., 2017; Israel, Papitto, et al., 2017; Rodríguez Castillo et al., 2020; Sathyaprakash, Roberts, Walton, Fuerst, et al., 2019) and sub-Eddington accreting IMBHs (Pasham et al., 2014).

The many long exposures expected in the course of a *LEM*-like mission would enable routine variability studies of all classes of X-ray sources, including ULXs. Such lightcurves would be uniformly sampled, which is important for minimizing biases due to the sampling pattern, as irregular sampling is known to distort the periodogram relative to the true PDS of the underlying variability process (e.g., Uttley, McHardy,

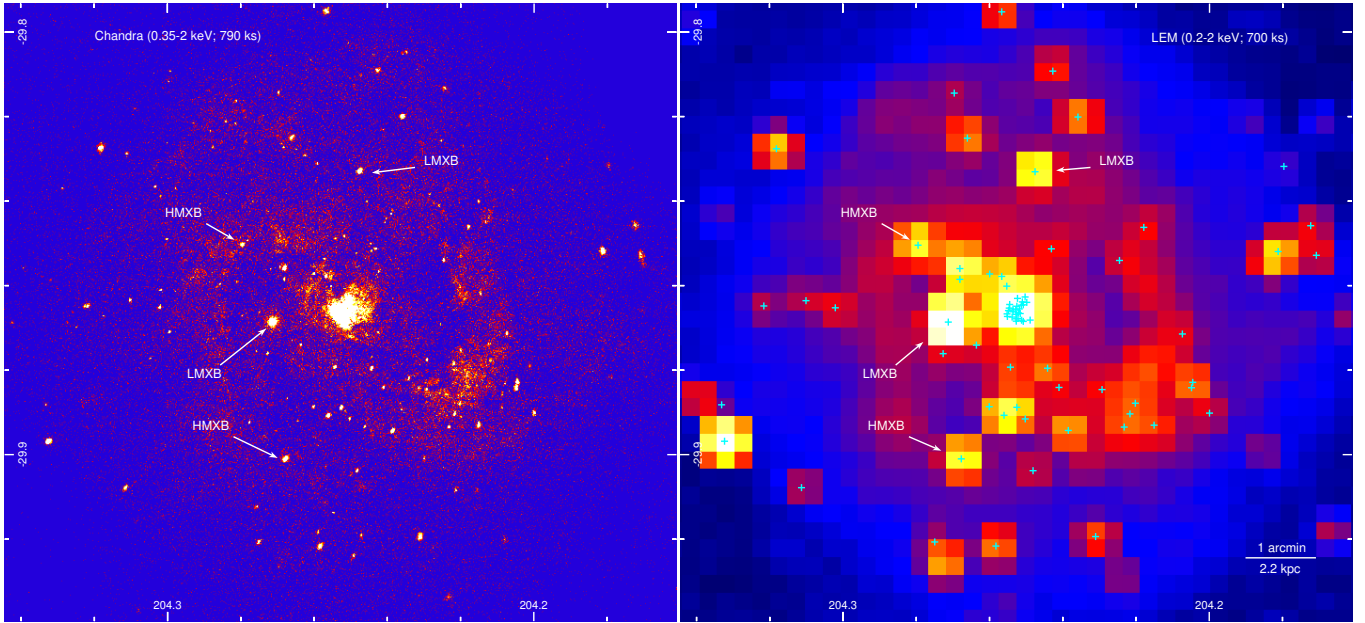


FIGURE 5 *Chandra* mosaic image (0.2–2 keV; 790 ks; left panel) and corresponding *LEM*-like simulated image (0.2–2 keV; 700 ks; right panel) of the same M83 field, based on luminous *Chandra* point sources (cyan crosses) and diffuse emission. Equatorial coordinates and logarithmic scaling are used. Numerous bright XRBs, several labeled, are clearly distinguished on the right.

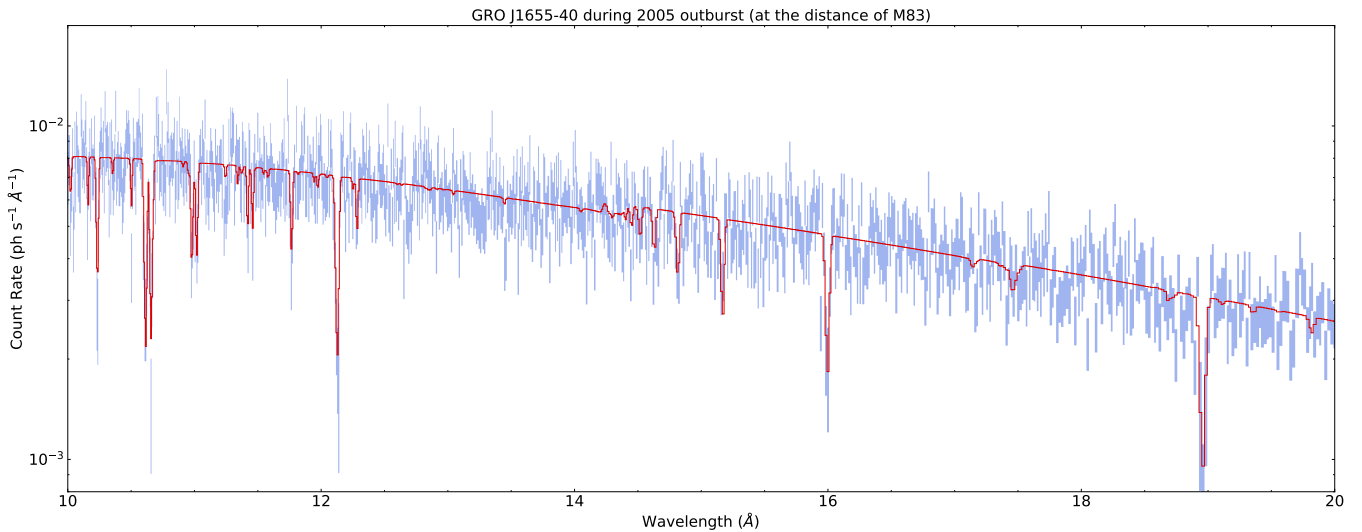


FIGURE 6 A *LEM*-like detector would permit the application of models that explore lines from the density and velocity of winds from the disks of bright XRBs situated in other galaxies. This is illustrated above which shows a simulated spectrum of an outbursting XRB similar to GRO J1655–40 placed at the distance of M83. The blue curve presents the spectrum (700 ks) simulated in SPEX (Kaastra et al., 1996) with optimal rebinning applied (Kaastra & Bleeker, 2016), and fit with the absorbed double-PION model from Tomaru et al. (2023) drawn in red. The wavelength range has been restricted to better highlight the spectral lines such as the Ne X α at 12.1 Å and the O VIII α (β) at 19 (16) Å.

& Papadakis, 2002; Vaughan, Edelson, Warwick, & Uttley, 2003). We adopt an instrumental time resolution of 1 millisecond, and accordingly a *LEM*-like instrument provides PDS

samples ~ 8 orders of magnitude in Fourier frequency, from $< 10^{-5}$ Hz for exposure times > 250 ks to the Nyquist frequency of ~ 500 Hz (with the PDS dominated by white noise

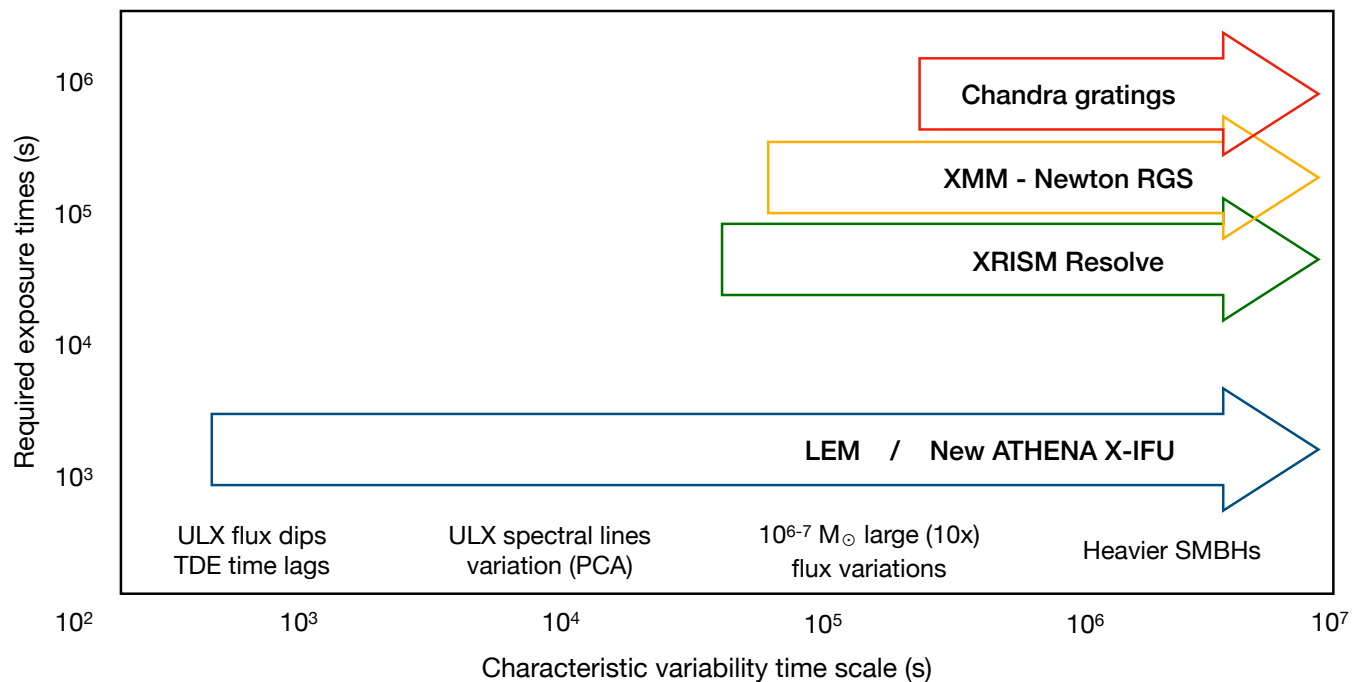


FIGURE 7 Shortest accessible timescales for a reference flux of $\sim 10^{-11} \text{ erg s}^{-1} \text{ cm}^{-2}$ which is a reasonable benchmark brightness for a ULX or X-ray bright TDE, using prospective high-spectral-resolution X-ray imagers compared to the present state-of-the-art. The exposure times describe line-detection thresholds for narrow oxygen K band (0.5 – 0.7 keV) features. Facilities like *LEM* and *Athena* offer comparable but complementary sensitivity, and are capable of reaching critical timescales in nearby ULXs. *LEM* offers a larger FOV (though with half-line sensitivity in its outer array) and is more capable for sources with softer spectra and most counts below 2 keV such as TDEs and soft-ULXs (SUL), whereas *NewAthena* is most capable for hard sources or much higher ionization.

at sufficiently-high frequencies, commonly by $\sim 0.1 - 10 \text{ Hz}$). The frequency of the high-frequency break in accreting BH PDS has been found to correlate with BH mass and mass accretion rate (McHardy, Koerding, Knigge, Uttley, & Fender, 2006). The accessible frequency range spans the breadth of PDS frequency breaks and QPOs associated with PULXs, BH and NS X-ray binaries, and IMBHs, potentially allowing differentiation between the various types of compact objects via timing directly. For instance, the high-frequency break of a ULX with a $400 M_{\odot}$ IMBH, such as that in M82 X-1 (Pasham et al., 2014), accreting at 0.1%-1% the Eddington rate is expected in the $\sim (0.02 - 0.2) \text{ Hz}$ frequency range.

Figure 8 shows simulated PDS corresponding to 250 ks observations with a *LEM*-like instrument of ULXs NGC 6946 X-1 and M82 X-1. Using spectral fits to these systems reported in Rao, Feng, and Kaaret (2010) and Brightman et al. (2020), the corresponding count rates are 0.6 cnt s^{-1} and 1.6 cnt s^{-1} , respectively. The broadband fractional rms variability and the QPO features were generated using values reported by Atapin, Fabrika, and Caballero-García (2019). These simulations demonstrate that the characteristic break frequencies,

as well as QPO characteristics, are readily recovered from galactic-field observations containing such systems.

5.2 | Elemental abundances and metal-enrichment insights from TDEs

More recent studies of ASASSN-14li suggest an overabundance of nitrogen in its photoionized wind is indicative of the disrupted star being moderately massive ($M \gtrsim 3 M_{\odot}$) with significant CNO processing. Alternatively, it may be that a lower-mass star was disrupted which had previously been stripped of its envelope (Miller et al., 2023). An accurate measurement of the individual absorption lines is of paramount importance within the context of evolution and metallicity, given that the latter can be very difficult to measure in galactic bulges.

Abundance diagnostics are likewise of central importance for XRB and ULX systems, in effort both to understand their stellar progenitors, and to reconcile an ongoing controversy in the field. Classical novae, i.e., cataclysmic variables often undergo a supersoft phase after a few dozens of days from the outburst and enable accurate measurements of elemental

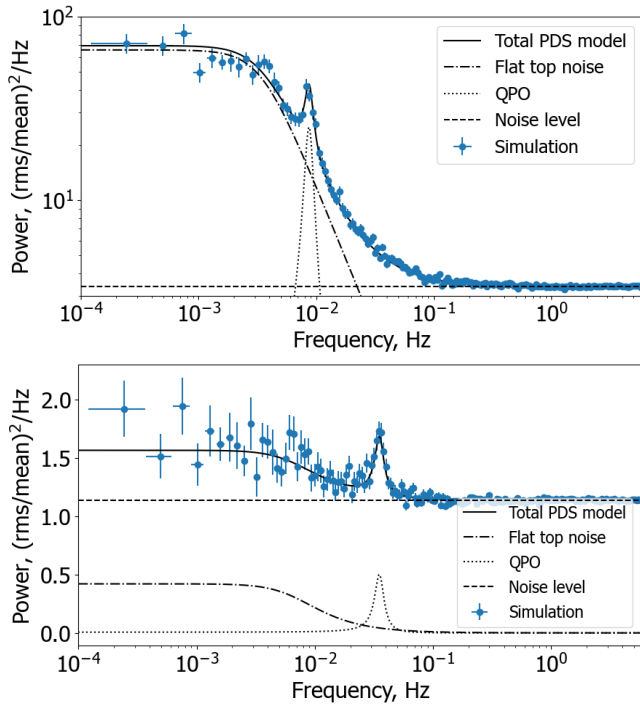


FIGURE 8 Simulated example PDS constructed from lightcurves simulated assuming a flat-top noise model with a characteristic break frequency, ν_b and a narrow QPO. The PDS is flat below the break, above which $\text{PDS} \propto \nu^{-\beta}$. These simulated data correspond to 250 ks observations with a *LEM*-like instrument using 30 ms time bins. The data were divided into 64 equal segments, with results averaged together and then logarithmically binned to improve the signal-to-noise ratio. The model PDS and fractional rms variability in the underlying lightcurves correspond to values reported for ULXs NGC 6946 X-1 (left) and M82 X-1 (right) in Atapin et al. (2019).

abundances which in an individual system provides unique identification of the donor-star’s nature (Ness et al., 2022; Pinto et al., 2012). Owing to their supersoft X-ray spectra and high luminosities (10^{38} erg s⁻¹), those in nearby galaxies within a few Mpc distance would yield useful abundance diagnostics from large-area, high-spectral-resolution X-ray studies. “Reflection” spectroscopic studies are widely used to measure BH spin and are based in models for reprocessed coronal emission on the disk’s surface-layer. These measurements consistently obtain a many-fold super-Solar abundance of Fe in XRB and AGN disk atmospheres (e.g., Tomsick et al. 2018). There are several candidate explanations, and here an independent assessment of elemental abundances via wind diagnostics will be revelatory for this debate.

5.3 | Disk structure and LOS effects at super-Eddington accretion rates

Most Galactic X-ray binaries emit at luminosities around or below the Eddington limit, $\sim 10^{39}$ erg/s for a typical $7-8 M_{\odot}$ BH. This corresponds to a mass accretion rate $\dot{M} \lesssim \dot{M}_{\text{Edd}} = L_{\text{Edd}}/\eta c^2 = 1.9 \times 10^{18} (M/M_{\odot}) \text{ g s}^{-1} = 2 \times 10^{-7} M_{\odot} \text{ yr}^{-1}$ assuming a radiative efficiency $\eta = 10\%$ typical for a weakly-spinning BH (with η varying from $\sim 6\%$ for a Schwarzschild BH to $\sim 40\%$ for a maximal Kerr BH). At higher accretion rates and, radiation pressure can surpass the gravitational pull, inflating the accretion disk vertically and launching powerful winds of ionized plasmas (Poutanen, Lipunova, Fabrika, Butkevich, & Abolmasov, 2007). These outflows can launch matter from the innermost region of the accretion disk where the escape velocity exceeds $0.1 c$ ($R \lesssim 100 R_G$). These are so-called ultrafast outflows (UFOs). Owing to the very soft SED of ULXs, their winds are expected to be only mildly ionized, $\log \xi \sim 2-4$ (e.g. Pinto, Mehdipour, et al. 2020), which indeed results in most of the absorption lines appearing in the soft X-ray bandpass (0.3-2 keV, e.g. Kosec et al. 2021) where a *LEM*-like observatory offers dramatic improvement in line sensitivity with respect to current instruments.

At $\dot{M} > \dot{M}_{\text{Edd}}$, the accretion disk becomes radiatively inefficient due to advection and photon trapping. The luminosity no longer grows linearly with mass-accretion rate, but instead transitions to a logarithmic scaling. At the same time, the inflated disk is geometrically thick, likely forming a funnel shape which can have the effect of collimating photons that are produced in the inner regions, scattering them upwards (also known as geometrical beaming). As a result, if such a system is seen face on, its luminosity would appear significantly boosted (A. R. King (2009), whereas its X-ray spectrum would become progressively softer (and weaker) at larger inclination angles (Middleton, Heil, et al., 2015). In principle, a near edge-on ULX may appear as simply an Eddington-limited XRB with either a supersoft spectrum (SSUL, e.g. Urquhart and Soria 2016) or else may be highly obscured in the most extreme cases such as the Galactic XRB SS 433 (Marshall, Canizares, and Schulz 2002).

5.3.1 | The relationship between winds and the underlying continuum

Owing to the funnel shape of the disk-wind cone, seen face-on, the wind is either absent or else highly ionized and the X-ray spectra would therefore appear hard, peaking between 2-10 keV (HUL, Sutton et al. 2013). Conversely, at large inclinations, optically-thick clumps of wind block X-ray photons originating in from the inner regions and the spectra appear softer and present strong absorption lines. Moreover, at increasingly high inclinations the wind that produces the absorption lines

should appear cooler and slower because it comes from the outer regions as suggested by theoretical simulations (Ohsuga, Mori, Nakamoto, and Mineshige 2005). These general predictions are favored by a 3σ correlation between the LOS velocity of the photoionized absorber and the hardness of the X-ray spectrum (defined as the ratio between the flux in the 1-10 keV band and the total 0.3-10 keV flux) measured for a small sample of ULXs with high-quality RGS spectra (Pinto, Mehdipour, et al. 2020). This is further supported by an anti-correlation between the hardness and the number of lines detected in the RGS spectra of a sample of 19 ULXs (Kosec et al., 2021).

We notice that funnel structure and the wind interaction with the X-ray photons produced in the inner accretion flow have been recently invoked for TDEs and some persistent highly-accreting SMBHs (mainly quasars and NLS1) where there is evidence for the wind to scatter X-rays thereby producing Fe K time lags (Kara, Miller, Reynolds, & Dai, 2016) and reflection features around 1 keV (Masterson et al., 2022) that could be resolved in a few cases through the RGS spectra (Xu et al., 2022). Moreover, there is a clear trend between the source X-ray luminosity and the wind properties in some AGN with the ionization and the velocity correlated with the source flux (Matzeu et al., 2017; Parker et al., 2017; Pinto, Mehdipour, et al., 2020; Xu et al., 2021, 2023). The study of **the wind response to the continuum requires effective area high enough ($\gtrsim 1000 \text{ cm}^2$) to enable tracking wind variability on small ($\lesssim 10\text{ks}$) timescales** and in this context a facility like the *LEM*-like design we have adopted for our simulations would be transformative.

5.4 | Black hole growth and feedback

Winds driven by strong radiation pressure in super-Eddington accretion disks achieve extreme velocities and are therefore expected to have a significant impact on the surrounding medium. This of course is expected both on the stellar-mass and supermassive (BH) scales. ULXs, for instance, are often surrounded by huge interstellar bubbles; this is also the case of the Galactic obscured source SS 433 (Broderick et al., 2018). Such bubbles are typically detected in the optical band where they exhibit strong emission lines from H α , He III and other species. The optical spectra of some bubbles are sensitive enough to constrain a supersonic expansion rate (80-250 km s⁻¹) and line-diagnostic ratios indicate mechanical expansion which is driven by outflows (Gúrpide et al., 2022). Their sizes (around 100 pc and larger) and ages (10^{5-6} yr) require a typical mechanical power of 10^{39-40} erg s⁻¹ (Pakull & Mirioni, 2002), which means that ULXs deposit huge amounts of energy into the surrounding ISM.

The outflow rate or the matter lost per unit of time in the wind can be expressed as $\dot{M}_w = 4\pi R^2 \rho v_w \Omega C$ where Ω and

C are the solid angle and the volume filling factor (or *clumpiness*), respectively, and R is the plasma distance from the source. The kinetic power of the winds is $L_w = 0.5 \dot{M}_w v_w^2 = 2\pi m_p \mu \Omega C L_{\text{ion}} v_w^3 / \xi$ where we used $\xi = L_{\text{ion}} / n_{\text{H}} R^2$. The largest uncertainties concern the solid angle and the clumpiness although modelling of P-Cygni profiles allows to place some constraints (see, e.g., the case of quasar PDS 456, Nardini et al. 2015). Alternative, observational, methods to estimate the solid angle rely on measuring the detection rate of winds in a statistical sample (e.g., Kosec et al. 2021; Tombesi et al. 2010). For ULXs, and more generally in XRBs, we are still missing such a statistically-robust sample owing to limitations in the current detectors. According to our simulations (see Fig. 1 to 4), a future *LEM*-like mission would facilitate spectroscopic studies of more distant and fainter sources as needed to obtain a critical sample.

A powerful technique to obtain tighter constraints on the outflow rate and other parameters uses the variability in the source luminosity. In particular, the higher the density of the ionized plasma, the faster its response to changes in the continuum. Many lines are sensitive to the plasma density, n_{H} , which allows to break its degeneracy with R , thereby constraining the launch radius (see e.g. TEPID and TPHO codes, Luminari, Nicastro, Krongold, Piro, and Linesh Thakur 2022; Rogantini et al. 2022). For such techniques, large effective area and high spectral resolution are both needed to track the wind response. This is challenging for current facilities but, as we showed in Figs. 1 and 3, readily feasible for a *LEM*-like observatory.

As mentioned in Sect. 1, TDEs or total disruptions of stars typically occur for BH masses $\lesssim 10^8 M_{\odot}$, and their peak accretion rates are thought to be highly super-Eddington (Wu et al., 2018). They are characterised by supersoft X-ray spectra ($kT_{\text{BB}} \sim 0.1$ keV). Given scale-invariance, our understanding of super-Eddington accretion by BHs in ULXs should broadly apply to SMBHs (although the cooler disks in AGN with respect to XRBs at the same L/L_{Edd} are more likely to drive strong winds via radiation pressure; Proga, Stone, and Kallman 2000; Quera-Bofarull et al. 2020), and outflows from super-Eddington phases of SMBH accretion may be an important source of feedback in cosmic evolution. Underscoring this relevance, general-relativistic magnetohydrodynamic simulations of super-Eddington SMBH accretion predict its viability and that it may be key to growing early SMBHs by enabling rapid BH growth on timescales $\lesssim 10^6$ yr (e.g., Ohsuga et al. 2005). However, observational confirmation is still needed to bolster this picture and assess its implications for the corresponding feedback which would be associated with early star formation.

6 | CONCLUSIONS

The small sample of ULXs with detections of absorption lines from the super-Eddington relativistic winds is limited by the effective area ($\lesssim 100 \text{ cm}^2$) of the current suite of high-spectral-resolution X-ray detectors in combination with the low fluence of extragalactic ULXs. Even those closest, within 10 Mpc have X-ray fluxes between 10^{-12} and $10^{-11} \text{ erg s}^{-1} \text{ cm}^{-2}$ requiring *XMM-Newton*/RGS exposures longer than 100 ks. Many ULXs are in crowded fields which hampers the capabilities of gratings instrument and of calorimeters with large PSF.

A next-generation mission offering large-FOV imaging in conjunction with high-spectral resolution would bring transformative capabilities for gaining insights into outflows in ULX and XRB populations in the local universe, and accordingly for probing changes in accretion-driven outflows from super-to-sub-Eddington regimes. Observations of nearby galaxies afford the important collateral capability of enabling hour-timescale dynamics of outflows in dozens of field sources.

There are roughly 10 ULXs with a flux comparable to NGC 1313 X-1 in the 0.5 – 2 keV band and a few dozen within a factor of a few (Walton et al., 2022). We therefore forecast that a *LEM*-like observatory would provide a dramatic, statistical, boost of the sample of ULXs with detections of mildly-relativistic winds (present census < 20 , and only ~ 10 with high significance) which would allow new constraints on the wind geometry, its outflow speed and kinetic energy. Most fundamentally, this would improve our understanding of the overall accretion mechanism and super-Eddington feedback.

The study of ULX winds on timescales shorter than ~ 10 ks is currently out of reach with grating spectrometers. With next-generational capabilities, an accurate measurement of the wind speed and outflow rate in the different flux regimes, and in particular during the dips, will confirm whether the radiation pressure (and therefore the local accretion rate) is increasing or decreasing, providing a definitive answer to this forefront question.

We have presented prospects for next-generational imaging-spectroscopy for the studies of outflows around compact objects and the physics of super-Eddington accretion around BHs ranging from XRBs to SMBHs, with TDEs as a bridge between super-Eddington and sub-Eddington regimes for SMBHs. Large area high-spectral resolution X-ray detectors are crucial to revealing outflow phenomena.

We demonstrate the important capability for next-generation X-ray facilities to provide robust and simultaneous detections of both slow (narrow) outflows, and relativistic ultra-fast outflows. With such instruments, it will additionally be possible to distinguish between collisional and photoionization models in understanding the drivers of winds as well as their impact

on the surrounding environment (e.g., as related to inflating 100 pc-scale bubbles observed surrounding ULXs).

ACKNOWLEDGMENTS

We acknowledge support from PRIN MUR 2022 SEAWIND 2022Y2T94C, INAF Large Grants 2023 BLOSSOM and Accordo Attuativo ASI-INAF n. 2019-27-HH.0 (ref. Luigi Piro). JFS acknowledges support from NuSTAR General Observer grant 80NSSC21K0078.

REFERENCES

- Alston, W. N., Pinto, C., Barret, D., D’Ai, A., Del Santo, M., et al. (2021, April), *MNRAS in press*, arXiv:2104.11163.
- Andreoni, I., Coughlin, M. W., Perley, D. A. et al. (2022, December), *Nature*, 612(7940), 430-434. doi:
- Atapin, K., Fabrika, S., & Caballero-García, M. D. (2019, June), *MNRAS*, 486(2), 2766-2779. doi:
- Auchettl, K., Guillochon, J., & Ramirez-Ruiz, E. (2017, April), *ApJ*, 838(2), 149. doi:
- Bañados, E., Venemans, B. P., Mazzucchelli, C. et al. (2018, January), *Nature*, 553(7689), 473-476. doi:
- Bachetti, M., Harrison, F. A., Walton, D. J., Grefenstette, B. W., Chakraborty, D., et al. (2014, October), *Nature*, 514, 202-204. doi:
- Bachetti, M., Rana, V., Walton, D. J., Barret, D., Harrison, F. A., et al. (2013, December), *ApJ*, 778, 163. doi:
- Barra, F., Pinto, C., Walton, D. J. et al. (2022, November), *MNRAS*, 516(3), 3972-3983. doi:
- Barret, D., Decourchelle, A., Fabian, A., Guainazzi, M., Nandra, K., Smith, R., & den Herder, J.-W. (2020, February), *Astronomische Nachrichten*, 341(2), 224-235. doi:
- Barret, D., Lam Trong, T., den Herder, J.-W., Piro, L., et al. (2018, Jul), The ATHENA X-ray Integral Field Unit (X-IFU). In SPIE Vol. 10699, p. 106991G. doi:
- Brightman, M., Kosec, P., Fürst, F. et al. (2022, April), *ApJ*, 929(2), 138. doi:
- Brightman, M., Walton, D. J., Xu, Y., Earnshaw, H. P., Harrison, F. A., Stern, D., & Barret, D. (2020, January), *ApJ*, 889(1), 71. doi:
- Broderick, J. W., Fender, R. P., Miller-Jones, J. C. A. et al. (2018, April), *MNRAS*, 475(4), 5360-5377. doi:
- Cackett, E. M., Bentz, M. C., & Kara, E. (2021, June), *iScience*, 24(6), 102557. doi:
- Carpano, S., Haberl, F., Maitra, C., & Vasilopoulos, G. (2018, May), *MNRAS*, 476, L45-L49. doi:
- Chakraborty, P., Ferland, G. J., Bianchi, S., & Chatzikos, M. (2020, October), *Research Notes of the American Astronomical Society*, 4(10), 184. doi:
- Chakraborty, P., Ferland, G. J., Chatzikos, M., Fabian, A. C., Bianchi, S., Guzmán, F., & Su, Y. (2022, August), *ApJ*, 935(2), 70. doi:
- Chakraborty, P., Ferland, G. J., Chatzikos, M., Guzmán, F., & Su, Y. (2020, September), *ApJ*, 901(1), 68. doi:
- Chakraborty, P., Ferland, G. J., Chatzikos, M., Guzmán, F., & Su, Y. (2021, May), *ApJ*, 912(1), 26. doi:
- Chatzikos, M., Bianchi, S., Camilloni, F. et al. (2023, August), *arXiv e-prints*, arXiv:2308.06396. doi:
- Coughlin, E. R., & Begelman, M. C. (2014, February), *ApJ*, 781(2), 82. doi:

- D'Ai, A., Pinto, C., Del Santo, M. et al. (2021, November), *MNRAS*, 507(4), 5567-5579. doi:
- Dai, L., McKinney, J. C., Roth, N., Ramirez-Ruiz, E., & Miller, M. C. (2018, June), *ApJ*, 859(2), L20. doi:
- Done, C., Wardziński, G., & Gierliński, M. (2004, April), *MNRAS*, 349(2), 393-403. doi:
- Fabian, A. C. (2012, September), *ARA&A*, 50, 455-489. doi:
- Fan, X., Bañados, E., & Simcoe, R. A. (2023, August), *ARA&A*, 61, 373-426. doi:
- Fan, X., Strauss, M. A., Schneider, D. P., Becker, R. H., White, R. L., et al. (2003, April), *AJ*, 125, 1649-1659. doi:
- Farrell, S. A., Webb, N. A., Barret, D., Godet, O., & Rodrigues, J. M. (2009, July), *Nature*, 460, 73-75. doi:
- Fender, R. P., Belloni, T. M., & Gallo, E. (2004, December), *MNRAS*, 355(4), 1105-1118. doi:
- Feng, H., Tao, L., Kaaret, P., & Grisé, F. (2016, November), *ApJ*, 831, 117. doi:
- Fürst, F., Walton, D. J., Harrison, F. A., et al. (2016, November), *ApJ*, 831, L14. doi:
- Gladstone, J. C., Copperwheat, C., Heinke, C. O., Roberts, T. P., Cartwright, T. F., Levan, A. J., & Goad, M. R. (2013, June), *ApJS*, 206(2), 14. doi:
- Gladstone, J. C., Roberts, T. P., & Done, C. (2009, August), *MNRAS*, 397, 1836-1851. doi:
- Goulding, A. D., Greene, J. E., Setton, D. J. et al. (2023, September), *ApJ*, 955(1), L24. doi:
- Guainazzi, M., & Tashiro, M. S. (2018, July), *ArXiv e-prints*.
- Guillochon, J., & Ramirez-Ruiz, E. (2013, April), *ApJ*, 767(1), 25. doi:
- Guillochon, J., & Ramirez-Ruiz, E. (2015, August), *ApJ*, 809(2), 166. doi:
- Guo, J., Sun, M., Gu, W.-M., & Yi, T. (2019, May), *MNRAS*, 485(2), 2558-2561. doi:
- Gürpide, A., Parra, M., Godet, O., Contini, T., & Olive, J. F. (2022, October), *A&A*, 666, A100. doi:
- Hammerstein, E., van Velzen, S., Gezari, S. et al. (2023, January), *ApJ*, 942(1), 9. doi:
- Heida, M., Lau, R. M., Davies, B. et al. (2019, October), *ApJ*, 883(2), L34. doi:
- Heil, L. M., Vaughan, S., & Roberts, T. P. (2009, August), *MNRAS*, 397, 1061-1072. doi:
- Hunt, Q., Gallo, E., Chandar, R., Johns Mulia, P., Mok, A., Prestwich, A., & Liu, S. (2021, May), *ApJ*, 912(1), 31. doi:
- Israel, G. L., Belfiore, A., Stella, L., Esposito, P., Casella, P., et al. (2017, February), *Science*, 355, 817-819. doi:
- Israel, G. L., Papitto, A., Esposito, P., Stella, L., Zampieri, L., et al. (2017, March), *MNRAS*, 466, L48-L52. doi:
- Jeon, J., Liu, B., Bromm, V., & Finkelstein, S. L. (2023, September), *MNRAS*, 524(1), 176-187. doi:
- Jiang, Y.-F., Stone, J. M., & Davis, S. W. (2019, August), *ApJ*, 880(2), 67. doi:
- Juodžbalis, I., Conselice, C. J., Singh, M. et al. (2023, October), *MNRAS*, 525(1), 1353-1364. doi:
- Kaaret, P., Prestwich, A. H., Zezas, A. et al. (2001, February), *MNRAS*, 321(2), L29-L32. doi:
- Kaastra, J. S., & Bleeker, J. A. M. (2016, March), *A&A*, 587, A151. doi:
- Kaastra, J. S., Mewe, R., & Nieuwenhuijzen, H. (1996), SPEX: a new code for spectral analysis of X & UV spectra. In K. Yamashita & T. Watanabe (Ed.), *UV and X-ray Spec. of Astr. and Lab. Plasmas* p. 411.
- Kalberla, P. M. W., Burton, W. B., Hartmann, D., Arnal, E. M., Bajaja, E., Morras, R., & Pöppel, W. G. L. (2005, September), *A&A*, 440, 775-782. doi:
- Kara, E., Dai, L., Reynolds, C. S., & Kallman, T. (2018, March), *MNRAS*, 474(3), 3593-3598. doi:
- Kara, E., Miller, J. M., Reynolds, C., & Dai, L. (2016, July), *Nature*, 535(7612), 388-390. doi:
- Kara, E., Pinto, C., Walton, D. J., Alston, W. N., Bachetti, M., et al. (2020, Feb), *MNRAS*, 491(4), 5172-5178. doi:
- Kelly, B. C., Becker, A. C., Sobolewska, M., Siemiginowska, A., & Uttley, P. (2014, June), *ApJ*, 788(1), 33. doi:
- King, A., Lasota, J.-P., & Middleton, M. (2023, June), *New A Rev.*, 96, 101672. doi:
- King, A. R. (2009, February), *MNRAS*, 393(1), L41-L44. doi:
- King, A. R., Davies, M. B., Ward, M. J., Fabbiano, G., & Elvis, M. (2001, May), *ApJ*, 552, L109-L112. doi:
- Kobayashi, H., Ohsuga, K., Takahashi, H. R., Kawashima, T., Asahina, Y., Takeuchi, S., & Mineshige, S. (2018, March), *PASJ*, 70, 22. doi:
- Komossa, S. (2015, September), *Journal of High Energy Astrophysics*, 7, 148-157. doi:
- Komossa, S., Voges, W., Xu, D. et al. (2006, August), *AJ*, 132(2), 531-545. doi:
- Kosec, P., Pasham, D., Kara, E., & Tombesi, F. (2023, September), *ApJ*, 954(2), 170. doi:
- Kosec, P., Pinto, C., Fabian, A. C., & Walton, D. J. (2018, February), *MNRAS*, 473, 5680-5697. doi:
- Kosec, P., Pinto, C., Reynolds, C. S. et al. (2021, December), *MNRAS*, 508(3), 3569-3588. doi:
- Kosec, P., Pinto, C., Walton, D. J., et al. (2018, September), *MNRAS*, 479, 3978-3986. doi:
- Kraft, R., Markevitch, M., Kilbourne, C. et al. (2022, November), *arXiv e-prints*, arXiv:2211.09827. doi:
- Lazzarini, M., Hornschemeier, A. E., Williams, B. F. et al. (2018, July), *ApJ*, 862(1), 28. doi:
- Lehmer, B. D., Eufrazio, R. T., Tzanavaris, P. et al. (2019, July), *ApJS*, 243(1), 3. doi:
- Lin, L. C.-C., Hu, C.-P., Li, K.-L. et al. (2020, February), *MNRAS*, 491(4), 5682-5692. doi:
- Long, K. S., Kuntz, K. D., Blair, W. P. et al. (2014, June), *ApJS*, 212(2), 21. doi:
- Luminari, A., Nicastro, F., Krongold, Y., Piro, L., & Linesh Thakur, A. (2022, December), *arXiv e-prints*, arXiv:2212.01399. doi:
- Marshall, H. L., Canizares, C. R., & Schulz, N. S. (2002, January), *ApJ*, 564(2), 941-952. doi:
- Masterson, M., Kara, E., Ricci, C. et al. (2022, July), *ApJ*, 934(1), 35. doi:
- Matzeu, G. A., Reeves, J. N., Braitto, V. et al. (2017, November), *MNRAS*, 472(1), L15-L19. doi:
- McHardy, I. M., Koerding, E., Knigge, C., Uttley, P., & Fender, R. P. (2006, December), *Nature*, 444(7120), 730-732. doi:
- Middleton, M. J., Heil, L., Pintore, F., Walton, D. J., & Roberts, T. P. (2015, March), *MNRAS*, 447, 3243-3263. doi:
- Middleton, M. J., Roberts, T. P., Done, C., & Jackson, F. E. (2011, February), *MNRAS*, 411, 644-652. doi:
- Middleton, M. J., Walton, D. J., Fabian, A., Roberts, T. P., Heil, L., Pinto, C., et al. (2015, December), *MNRAS*, 454, 3134-3142. doi:
- Miller, J. M., Fabbiano, G., Miller, M. C., & Fabian, A. C. (2003, March), *ApJ*, 585(1), L37-L40. doi:
- Miller, J. M., Kaastra, J. S., Miller, M. C. et al. (2015, October), *Nature*, 526(7574), 542-545. doi:
- Miller, J. M., Mockler, B., Ramirez-Ruiz, E. et al. (2023, August), *ApJ*, 953(2), L23. doi:
- Miller, J. M., Raymond, J., Fabian, A. C. et al. (2016, April), *ApJ*, 821(1), L9. doi:
- Miller, J. M., Raymond, J., Reynolds, C. S., Fabian, A. C., Kallman,

- T. R., & Homan, J. (2008, June), *ApJ*, 680(2), 1359-1377. doi: Mizumoto, M., Nomura, M., Done, C., Ohsuga, K., & Odaka, H. (2021, May), *MNRAS*, 503(1), 1442-1458. doi:
- Nardini, E., Reeves, J. N., Gofford, J. et al. (2015, February), *Science*, 347(6224), 860-863. doi:
- Neilsen, J., & Lee, J. C. (2009, March), *Nature*, 458, 481-484. doi:
- Ness, J. U., Beardmore, A. P., Bezak, P. et al. (2022, February), *A&A*, 658, A169. doi:
- Ohsuga, K., Mori, M., Nakamoto, T., & Mineshige, S. (2005, July), *ApJ*, 628, 368-381. doi:
- Pakull, M. W., Gris e, F., & Motch, C. (2006), Ultraluminous X-ray Sources: Bubbles and Optical Counterparts. In E. J. A. Meurs & G. Fabbiano (Eds.), *Populations of High Energy Sources in Galaxies* Vol. 230, p. 293-297. doi:
- Pakull, M. W., & Mirioni, L. (2002, February), *arXiv Astrophysics e-prints*.
- Parker, M. L., Pinto, C., Fabian, A. C., Lohfink, A., Buisson, D. J. K., et al. (2017, March), *Nature*, 543, 83-86. doi:
- Parker, M. L., Reeves, J. N., Matzeu, G. A., Buisson, D. J. K., & Fabian, A. C. (2018, February), *MNRAS*, 474(1), 108-114. doi:
- Pasham, D. R., Remillard, R. A., Fragile, P. C. et al. (2019, February), *Science*, 363(6426), 531-534. doi:
- Pasham, D. R., Strohmayer, T. E., & Mushotzky, R. F. (2014, September), *Nature*, 513(7516), 74-76. doi:
- Pasham, D. R., & van Velzen, S. (2018, March), *ApJ*, 856(1), 1. doi:
- Pinto, C., Alston, W., Soria, R., Middleton, M. J., Walton, D. J., et al. (2017, July), *MNRAS*, 468, 2865-2883. doi:
- Pinto, C., Kaastra, J. S., Costantini, E., & de Vries, C. (2013, March), *A&A*, 551, A25. doi:
- Pinto, C., Mehdipour, M., Walton, D. J., Middleton, M. J., Roberts, T. P., et al. (2020, February), *MNRAS*, 491(4), 5702-5716. doi:
- Pinto, C., Middleton, M. J., & Fabian, A. C. (2016, May), *Nature*, 533, 64-67. doi:
- Pinto, C., Ness, J.-U., Verbunt, F., Kaastra, J. S., Costantini, E., & Detmers, R. G. (2012, July), *A&A*, 543, A134. doi:
- Pinto, C., Soria, R., Walton, D. J. et al. (2021, August), *MNRAS*, 505(4), 5058-5074. doi:
- Pinto, C., & Walton, D. J. (2023, January), *arXiv e-prints*, arXiv:2302.00006. doi:
- Pinto, C., Walton, D. J., Kara, E., Parker, M. L., Soria, R., et al. (2020, March), *MNRAS*, 492(4), 4646-4665. doi:
- Pintore, F., Motta, S., Pinto, C. et al. (2021, June), *MNRAS*, 504(1), 551-564. doi:
- Pintore, F., Zampieri, L., Stella, L., Wolter, A., Mereghetti, S., & Israel, G. L. (2017, February), *ApJ*, 836, 113. doi:
- Ponti, G., Fender, R. P., Begelman, M. C., Dunn, R. J. H., Neilsen, J., & Coriat, M. (2012, May), *MNRAS*, 422, L11-L15. doi:
- Poutanen, J., Lipunova, G., Fabrika, S., Butkevich, A. G., & Abolmasov, P. (2007, May), *MNRAS*, 377, 1187-1194. doi:
- Proga, D., Stone, J. M., & Kallman, T. R. (2000, November), *ApJ*, 543, 686-696. doi:
- Psaradaki, I., Costantini, E., Mehdipour, M., & D az Trigo, M. (2018, December), *A&A*, 620, A129. doi:
- Psaradaki, I., Costantini, E., Rogantini, D. et al. (2023, February), *A&A*, 670, A30. doi:
- Quera-Bofarull, A., Done, C., Lacey, C., McDowell, J. C., Risaliti, G., & Elvis, M. (2020, June), *MNRAS*, 495(1), 402-412. doi:
- Rao, F., Feng, H., & Kaaret, P. (2010, October), *ApJ*, 722(1), 620-624. doi:
- Rappaport, S. A., Podsiadlowski, P., & Pfahl, E. (2005, January), *MNRAS*, 356(2), 401-414. doi:
- Rees, M. J. (1988, June), *Nature*, 333(6173), 523-528. doi:
- Remillard, R. A., & McClintock, J. E. (2006, September), *ARA&A*, 44(1), 49-92. doi:
- Robba, A., Pinto, C., Pintore, F., et al. (2021, August), *A&A*, 652, 16. doi:
- Rodr guez Castillo, G. A., Israel, G. L., Belfiore, A. et al. (2020, May), *ApJ*, 895(1), 60. doi:
- Rogantini, D., Mehdipour, M., Kaastra, J., Costantini, E., Jur anova, A., & Kara, E. (2022, December), *ApJ*, 940(2), 122. doi:
- Sadowski, A., Narayan, R., McKinney, J. C., & Tchekhovskoy, A. (2014, March), *MNRAS*, 439(1), 503-520. doi:
- Sathyaprakash, R., Roberts, T. P., Walton, D. J., Fuerst, F., et al. (2019, Jul), *MNRAS*, L104. doi:
- Sazonov, S., Gilfanov, M., Medvedev, P. et al. (2021, December), *MNRAS*, 508(3), 3820-3847. doi:
- Schellenberger, G., Bogdan, ., ZuHone, J. A. et al. (2023, July), *arXiv e-prints*, arXiv:2307.01259. doi:
- Smith, R. K., Bautz, M., Bregman, J. et al. (2022, August), Arcus: exploring the formation and evolution of clusters, galaxies, and stars. In J.-W. A. den Herder, S. Nikzad, & K. Nakazawa (Eds.), *Space Telescopes and Instrumentation 2022: Ultraviolet to Gamma Ray* Vol. 12181, p. 1218121. doi:
- Steiner, J. F., McClintock, J. E., Remillard, R. A., Gou, L., Yamada, S., & Narayan, R. (2010, August), *ApJ*, 718(2), L117-L121. doi:
- Stobbart, A.-M., Roberts, T. P., & Wilms, J. (2006, May), *MNRAS*, 368, 397-413. doi:
- Sutton, A. D., Roberts, T. P., & Middleton, M. J. (2013, October), *MNRAS*, 435, 1758-1775. doi:
- Sutton, A. D., Roberts, T. P., & Middleton, M. J. (2015, November), *ApJ*, 814, 73. doi:
- Tomaru, R., Done, C., & Mao, J. (2023, January), *MNRAS*, 518(2), 1789-1801. doi:
- Tombesi, F., Cappi, M., Reeves, J. N., Palumbo, G. G. C., Yaqoob, T., Braito, V., & Dadina, M. (2010, October), *A&A*, 521, A57. doi:
- Tomsick, J. A., Parker, M. L., Garc a, J. A. et al. (2018, March), *ApJ*, 855(1), 3. doi:
- Urquhart, R., & Soria, R. (2016, February), *MNRAS*, 456, 1859-1880. doi:
- Uttley, P., McHardy, I. M., & Papadakis, I. E. (2002, May), *MNRAS*, 332(1), 231-250. doi:
- van den Eijnden, J., Degenaar, N., Schulz, N. S. et al. (2019, August), *MNRAS*, 487(3), 4355-4371. doi:
- van Velzen, S., Farrar, G. R., Gezari, S. et al. (2011, November), *ApJ*, 741(2), 73. doi:
- Vaughan, S., Edelson, R., Warwick, R. S., & Uttley, P. (2003, November), *MNRAS*, 345(4), 1271-1284. doi:
- Volonteri, M., Silk, J., & Dubus, G. (2015, May), *ApJ*, 804(2), 148. doi:
- Walton, D. J., Mackenzie, A. D. A., Gully, H., Patel, N. R., Roberts, T. P., Earnshaw, H. P., & Mateos, S. (2022, January), *Monthly Notices of the Royal Astronomical Society*, 509, 1587-1604. doi:
- Walton, D. J., Middleton, M. J., Pinto, C., Fabian, A. C., Bachetti, M., et al. (2016, August), *ApJ*, 826, L26. doi:
- Walton, D. J., Pinto, C., Nowak, M. et al. (2020, June), *MNRAS*, 494(4), 6012-6029. doi:
- Wang, J., Fabbiano, G., Elvis, M. et al. (2011, November), *ApJ*, 742(1), 23. doi:
- Wang, Q. D., Zeng, Y., Bogdan, ., & Ji, L. (2021, December), *MNRAS*, 508(4), 6155-6175. doi:
- Wiktorowicz, G., Lasota, J.-P., Belczynski, K., Lu, Y., Liu, J., & Hkiewicz, K. (2021, September), *ApJ*, 918(2), 60. doi:
- Wiktorowicz, G., Sobolewska, M., Sadowski, A., & Belczynski, K. (2015, September), *ApJ*, 810(1), 20. doi:
- Wilson-Hodge, C. A., Malacaria, C., Jenke, P. A. et al. (2018, August), *ApJ*, 863(1), 9. doi:
- Wu, S., Coughlin, E. R., & Nixon, C. (2018, August), *MNRAS*, 478(3), 3016-3024. doi:

- XRISM Science Team. (2020, March), *arXiv e-prints*, arXiv:2003.04962. doi:
- Xu, Y., Pinto, C., Bianchi, S. et al. (2021, December), *MNRAS*, 508(4), 6049-6067. doi:
- Xu, Y., Pinto, C., Kara, E. et al. (2022, June), *MNRAS*, 513(2), 1910-1924. doi:
- Xu, Y., Pinto, C., Rogantini, D. et al. (2023, August), *MNRAS*, 523(2), 2158-2171. doi:
- Zhou, C., Feng, H., & Bian, F. (2023, June), *arXiv e-prints*, arXiv:2306.06810. doi:

How cite this article: C. Pinto, J. F. Steiner, A. Bodaghee, P. Chakraborty, M. Sobolewska et al. (2024), Probing extreme black-hole outflows on short timescales via high spectral-resolution X-ray imagers, *Astron. Nachr. / AN.*, 2024;00:X–Y.

How cite this article: C. Pinto, J. F. Steiner, A. Bodaghee, P. Chakraborty, M. Sobolewska et al. (2024), Probing extreme black-hole outflows on short timescales via high spectral-resolution X-ray imagers, *Astron. Nachr. / AN.*, 2024;00:X–Y.